International Journal of Mechanical Sciences 65 (2012) 125–133

Contents lists available at SciVerse ScienceDirect

International Journal of Mechanical Sciences

journal homepage: www.elsevier.com/locate/ijmecsci

Design of nonlinear impact dampers based on acoustic and damping behavior

Aref Afsharfard *, Anooshiravan Farshidianfar

Department of Mechanical Engineering, Ferdowsi University of Mashhad, Mashhad, Iran

ARTICLE INFO

Article history:
Received 6 August 2011
Received in revised form
18 August 2012
Accepted 12 September 2012
Available online 1 October 2012

Keywords:
Impact damper
Hertzian contact
Acoustic theory
Nonlinear differential equation

ABSTRACT

In the present study, mathematical model of the sound radiated from an impact oscillator that incorporates the Hertzian contact is analyzed. Transient sound generated from the contact of a sphere with a reflecting plane is obtained theoretically and it is compared with the previous experimental results. The acoustic noise radiated from a spherical mass colliding with a wall–floor intersection is obtained using the method of images. This method is used to predict the acoustic noise generated by a single unit impact damper. A nonlinear model is developed to investigate the effect of mass ratio, coefficient of restitution and gap size on behavior of the single unit impact damper. Finally, damping and acoustic behavior of the impact damper are illustrated in a user-oriented diagram to find a low noise system, which can strongly suppress the undesired vibrations.

1. Introduction

One of the most important sources of noise is impulsive sources because impact occurs in many mechanical devices. Models of vibro-impact systems are widely used in vibration engineering, structural mechanics etc. The reaction forces during a collision and the dynamic response of structures to these reaction forces are widely investigated experimentally and analytically [1,2].

Considerable research is generally done on the theory of sound radiation but impact noise in practical applications is an area, which has received little attention. One of the relatively new sources of the impact noise, as found in industry, is those caused by single unit impact dampers (or simply impact dampers). It is shown that the impact dampers can operate more efficiently than classical dynamic vibration dampers [3]. Impact dampers can extensively be used to attenuate undesired vibration of robot arms, turbine blades and so on [4,5]. Behavior of impact dampers have been investigated experimentally, analytically and numerically for many years [6–8]. It is shown that performance of an impact damper in free damped vibration is strongly depends on the clearance between the impact mass and main mass (gap size). Cheng and Wang indicated that the gap should be smaller than twice of the initial displacement of the main mass in free damped vibrations [9]. Coefficient of restitution and the mass ratio have great effects on the application of impact dampers [6]. Cheng and Xu obtained a relation between coefficient of restitution and impact damping ratio [5]. Du and Wang showed that the fine particle impact dampers using plastic deformation of fine particles can exhaust much more vibration energy than usual single unit impact dampers and thus can work well in low frequency domain [10].

Although application of the impact dampers has been investigated for a long time, there are still several shortcomings in this area of research that should be noticed.

- Although vibro-impact systems often exhibit strongly nonlinear behavior [11], there is a tendency to describe them by linear equations.
- In reality, coefficient of restitution varies with changing the contact parameters. Usually, for convenience, this parameter is considered as a constant value.
- Effects of changing mass ratio, coefficient of restitution and gap size on behavior of a vibratory system equipped with an impact damper are widely investigated. This area of research can be developed by investigating the acoustic behavior of impact dampers.

The main target of the present work is to analyze the nonlinear behavior of a vibratory system equipped with an impact damper and optimize the results with the acoustical considerations. In the present work, contact force acting between the mass colliding with barrier is defined using the Hertzian contact theory [2,12]. The variable coefficient of restitution, which varies with the mass ratio, is theoretically achieved using the Newmark-beta

* Corresponding author. Tel.: +98 511 8695553; fax: +98 511 8763304.
E-mail addresses: aref.afsharfard@stu-mail.um.ac.ir, aref.afsharfard@gmail.com (A. Afsharfard).

0020-7403/$ - see front matter © 2012 Elsevier Ltd. All rights reserved.
http://dx.doi.org/10.1016/j.ijmecsci.2012.09.010

Nomenclature

a	Radius of the sphere
C	Viscous damping
c	Wave propagation velocity
c_1	Equivalent contact damping constant for an impact damper
DI	Directivity index
d	Gap size
E	Young's modulus
e	Damping inclination
K	Linear stiffness
K_{HZ}	Hertzian contact stiffness
L_W	Sound power
M	Main mass
m	Impact mass
p	Acoustic pressure
R	Coefficient of restitution
r	Distance to measurement position
SPL	Sound pressure level
T_d	Time delay
U_0	Contact velocity amplitude
z	Relative displacement, $z=y-x$
ω	Angular frequency
ϕ	Potential velocity
δ	Dirac delta function
τ	Contact duration
ν	Poisson's ratio
α	Value of the approach

integration method. The calculated results are compared and verified using the previous exact results. Furthermore, to improve the initial design of the impact dampers, the acoustical behavior of these systems is accounted.

The classical theory of the acoustic noise radiated from vibratory bodies has been developed in detail for the harmonic steady-state case [13]. Kirchhoff derived the radiation field generated by an impulsive translational acceleration of a sphere. Koss and Alfredson inferred the functional relation between the sound pressure of the impact of balls and time [14]. Akay and Hodgson presented a theoretical derivation of the sound pressure waveform for an elastic impact of a sphere with a massive slab [15]. Yufang and Zhongfang investigated the radiation of acoustical noise from impact of two cylinders [16].

In the present study, the acoustic field radiated from the sphere subjected to an impulsive Hertzian acceleration is obtained using the convolution integral technique. The complete sound field, radiated from dipole and quadrupole sources, is achieved by employing the method of images where the impact mass and its images are treated as independent transient sound sources. The theoretical results are verified by previous experimental measurements. The effects of the mass ratio, the coefficient of restitution and the gap size are investigated on the free vibration of a vibratory system with an impact damper. Furthermore, the maximum sound pressure level that is generated by the impact damper is obtained and analyzed. The initial design of an impact damper, in the present study, is divided to acoustic-based and vibration-based designs. Finally, the vibration-based and acoustic-based results are collected in a user-oriented chart to find the best selection for the mass ratio and gap size to have a low-noise system, which strongly attenuates undesired vibrations.

2. Mechanics of impact

In the present study, contact of a sphere with a reflecting plane is described using the Hertz theory. The Hertzian contact is based on the assumption that the elastic energy acquired by the colliding bodies during impact is entirely reversible. For an elastic impact, the body deformation is localized and the corresponding energy losses can be assumed negligible. The expression for the contact force according to the Hertzian model is as follows [11,17]:

$$F_{HZ} = K_{HZ}\alpha^{3/2} \tag{1}$$

where α is the relative displacement of colliding bodies (value of the approach) and K_{HZ} is the Hertzian contact stiffness which can be obtained using the following relation [15]:

$$K_{HZ} = \frac{4}{3\pi}\frac{\sqrt{a}}{(1-\nu_1^2)/\pi E_1 + (1-\nu_2^2)/\pi E_2} \tag{2}$$

where ν is the Poisson's ratio, E is the Young's modulus, a is the radius of the sphere and subscripts 1 and 2 refer to the sphere and the slab, respectively. From Newton's law, the following differential equation can be concluded [16]:

$$\ddot{\alpha} = -K^* K_{HZ}\alpha^{3/2};\ \ \alpha(0)=0,\ \ \dot{\alpha}(0)=U_0 \tag{3}$$

where U_0 is the contact velocity amplitude, m is the mass of the colliding sphere and $K^*=1/m$. According to the above differential equation, It is evident that:

$$\frac{1}{2}\left(\dot{\alpha}^2 - U_0^2\right) = -\frac{2}{5}K^* K_{HZ}\alpha^{5/2} \tag{4}$$

It is obvious that the maximum deformation occurs when $\dot{\alpha}=0$, so it can be written as follows:

$$\alpha_{\max} = \left(\frac{5U_0^2}{4K^* K_{HZ}}\right)^{2/5} \tag{5}$$

Maximum value of the contact force occurs when $\alpha=\alpha_{\max}$. Therefore, according to the Hertzian contact and the Newton's second law of motion, the maximum acceleration of the impacting mass is equal to:

$$A_{\max} = \frac{K_{HZ}}{m}\left(\frac{5U_0^2}{4K^* K_{HZ}}\right)^{3/5} \tag{6}$$

Hence, the impact acceleration of the impact mass is as follows:

$$A(t) = A_{\max}\sin\left(\frac{\pi t}{\tau}\right) \tag{7}$$

where τ is the contact duration and it is equal to $\tau = 2.9432\alpha_{\max}/U_0$ [16]. It should be noted that all of the presented relations, to here, are valid if the slab is fixed. In the case of movable slabs (for example, in the case of impact dampers), based on the Newton's second law, the impact force acting on each of the colliding bodies is equal to:

$$F = -m\ddot{w}_1 = -M\ddot{w}_2 = -\frac{mM}{m+M}\ddot{\alpha} \tag{8}$$

In the above relation, $\ddot{w}_1+\ddot{w}_2=\ddot{\alpha}$, furthermore, M and m is the moveable slab mass (main mass) and the impact mass, respectively. Therefore, it can be concluded that for the movable slabs, the parameter K^* (in Eqs. (4) and (5)) is equal to $K^*=(m+M)/(m.M)$.

3. Acoustic theory

Consider a sphere (which travels with an initial velocity) collides with a reflecting wall. For the impact situation, the centre of the sphere was chosen as the centre of a spherical coordinate system. The sound field can be described by [18]:

$$u=\frac{\partial\phi}{\partial r} \tag{9}$$

where u is particle velocity and ϕ is a potential velocity. The wave equation is as follows [18]:

$$\frac{\partial^2(r\phi)}{\partial r^2}=\frac{1}{c^2}\frac{\partial^2(r\phi)}{\partial t^2} \tag{10}$$

where c is the wave propagation velocity. The velocity potential generated by an oscillating sphere of radius a is shown in following relation [14]:

$$\phi(r,t,\theta)=\frac{a^3v}{r^2}\frac{(1+jkr)\cos\theta}{2(1+jka)-(ka)^2}\exp(j\omega t-jk(r-a)) \tag{11}$$

where k is the wave number and it is equal to ω/c, ω is the angular frequency of oscillation, θ is the polar angle, j is the positive root of minus one and v is the velocity amplitude. The velocity of the sphere due to a unit impulse of acceleration can be written as follows [14]:

$$v(\omega)=\pi\delta(\omega)+\frac{j}{\omega} \tag{12}$$

where δ is the Dirac delta function. The velocity potential for an arbitrary velocity $v(\omega)$ can be achieved, using Fourier synthesis [19], as follows:

$$\phi(r,t,\theta)=\frac{a^3\cos\theta}{r^2}\int_{-\infty}^{+\infty}v(\omega)(1+jkr)\exp\left(\frac{j\omega t-jk(r-a))}{2(1+jka)-(ka)^2}d\omega\right. \tag{13}$$

The solution of the above relation is evaluated using contour integration in the complex plane. It is shown as follows:

$$\phi(r,t,\theta)=\frac{a^3\cos\theta}{2r^2}\left\{\left[\left(\frac{2r}{a}-1\right)\sin(lt')-\cos(lt')\right]\exp(-lt')+1\right\} \tag{14}$$

where $t'=t-(r-a)/c$ and $l=c/a$. Therefore, the acoustic pressure, which is equal to $p=\rho_0(\partial\phi/\partial t')$, can be written as follows:

$$p=\rho_0c\frac{a^2\cos\theta}{r^2}\left\{\left(1-\frac{r}{a}\right)\sin(lt')+\left(\frac{r}{a}\right)\cos(lt')\right\}\exp(-lt') \tag{15}$$

The acoustic pressure radiated from a sphere subjected to an arbitrary acceleration $A(t)$ can be calculated by the convolution technique [18] where:

$$p=\int_0^B p(t'-\xi)A(\xi)d\xi \tag{16}$$

The ξ in the above relation is the integration variable. Substituting Eqs. (7) and (15) into Eq. (16) results in:

$$p=\left(\rho_0c\frac{a^2}{r^2}\cos\theta\right)\left(\frac{125}{64}\frac{K_{HZ}^2U_0^6}{m^2}\right)^{1/5}\int_0^B(1-r/a)\sin(l(t'-\xi))+(r/a)\cos(l(t'-\xi))\}\exp(-l(t'-\xi))\sin\left(\frac{\pi\xi}{d}\right)d\xi \tag{17}$$

The above integral should be evaluated for two different time intervals because the Hertzian acceleration exists for only a finite period. Therefore, $B=t'$ when $0\le t'\le\tau$ and $B=\tau$ when $t'>\tau$. For time intervals $0\le t'\le\tau$, the acoustic pressure is equal to [15]:

$$p_I=\frac{\rho_0ca\cos\theta}{2r}(C_1/C_2)\{C_3\sin(\pi t'/\tau)-C_5\cos(\pi t'/\tau)-(1-(a/r))[C_4\sin(\pi t'/\tau)-C_6\cos(\pi t'/\tau)]+[C_5\cos(ct'/a)-C_6\sin(ct'/a)]\exp(-ct'/a)-(1-(a/r))[C_6\cos(ct'/a)+C_5\sin(ct'/a)]\exp(-ct'/a)\} \tag{18}$$

and for time intervals $t'>\tau$ the acoustic pressure can be formulated as follows:

$$p_{II}=\frac{\rho_0ca\cos\theta}{2r}(C_1/C_2)\{[C_5\cos(ct'/a)-C_6\sin(ct'/a)]\exp(-ct'/a)-[C_6\sin(c(t'-\tau)/a)-C_5\cos(c(t'-\tau)/a)]\exp(-c(t'-\tau)/a)-(1-(a/r))[C_6\cos(ct'/a)+C_5\sin(ct'/a)]\exp(-ct'/a)+(1-(a/r))[C_4\sin(c(t'-\tau)/a)-C_6\cos(c(t'-\tau)/a)]\exp(-c(t'-\tau)/a) \tag{19}$$

where the coefficients C_1 to C_6 are:

$$C_1=A_{\max}\quad C_2=4(c/a)^4+(\pi/\tau)^4$$
$$C_3=4(c/a)^3+2(\pi/\tau)^2(c/a)\quad C_4=4(c/a)^3-2(\pi/\tau)^2(c/a)$$
$$C_5=2(\pi/\tau)^3\quad C_6=4(\pi/\tau)(c/a)^2$$

Presence of the reflecting plane can be accounted by employing the method of images [20]. Deformation of the sphere and reflecting plane can be neglected during the sound radiation because the pressure pulse duration is only a small multiple of the contact duration. Therefore, the source can be assumed as a dipole type source and its image oppose each other, as shown in Fig. 1. The resulting pressure at the field point p is then [20]:

$$p(r,\theta,t)=p(r_1,\theta_1,t_1)-p(r_2,\theta_2,t_2) \tag{20}$$

Parameters r_1, r_2, θ_1 and θ_2 are calculated by:

$$r_1=\sqrt{r^2+a^2-2ar\cos\theta}\quad\theta_1=\cos^{-1}((r\cos\theta-a)/r_1)$$
$$r_2=\sqrt{r^2+a^2+2ar\cos\theta}\quad\theta_2=\cos^{-1}((r\cos\theta+a)/r_2)$$

The pressure waves generated by the spherical mass and its image do not arrive simultaneously at every spatial position r, θ. The time delay between the sound waves is assumed to be [14]:

$$T_d=\frac{|r_2-r_1|}{c} \tag{21}$$

Variables t_1 and t_2 in Eq. (20) have the relation $t_1=t_2+T_d$. The total sound pressure wave can be obtained by substituting Eqs. (18) and (19) into Eq. (20). A calculation of the pressure waveform for the impact of spherical mass with barrier is shown in Fig. 2. Furthermore, for verifying, previous published result [15]

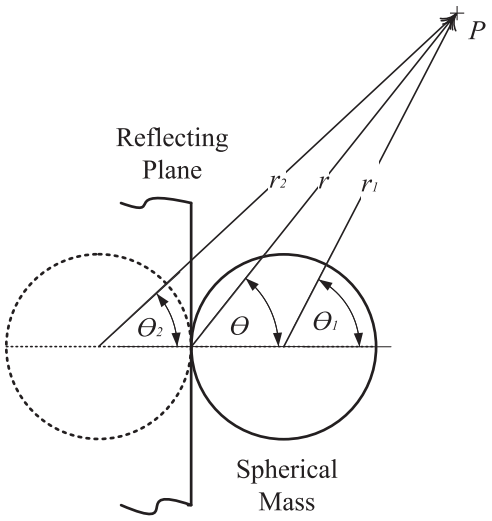

Fig. 1. Dipole and its image representation.

is illustrated in this figure. This waveform is characteristically M-shaped, with a larger negative pressure peak than the two positive values.

The sound pressure level of the acoustic noise radiated from the dipole is calculated circumferentially around the contact point. The directivity pattern for the dipole source is shown in Fig. 3. In Table 1, the theoretically measured values of the sound pressure levels are compared with the corresponding experimental results [15].

In many real engineering cases (for example, in the case of impact dampers), the acoustical source is situated near two hard reflecting planes (wall–floor intersection). Therefore, the source must be assumed as a quadrupole type source, as shown in Fig. 4.

In the case of the quadrupole sources, result pressure at the field point can be written as follows:

$$p(r,\theta,t)=p(r_1,\theta_1,t_1)-p(r_2,\theta_2,t_2)+p(r_3,\theta_3,t_3)-p(r_4,\theta_4,t_4) \quad (22)$$

Where

$$r_1=\sqrt{r^2+a^2-2ar\cos\theta} \quad \cos\theta_1=(r\cos\theta-a)/r_1 \quad \sin\theta_1=(r\sin\theta)/r_1$$

$$r_2=\sqrt{r^2+a^2+2ar\cos\theta} \quad \cos\theta_2=(r\cos\theta+a)/r_2 \quad \sin\theta_2=(r\sin\theta)/r_2$$

$$r_3=\sqrt{r_2^2+4a^2+4ar_2\sin\theta_2} \quad \cos\theta_3=(r\cos\theta+a)/r_3 \quad \sin\theta_3=(r\sin\theta+2a)/r_3$$

$$r_4=\sqrt{r_1^2+4a^2+4ar_1\sin\theta_1} \quad \cos\theta_4=(r\cos\theta-a)/r_4 \quad \sin\theta_4=(r\sin\theta+2a)/r_4$$

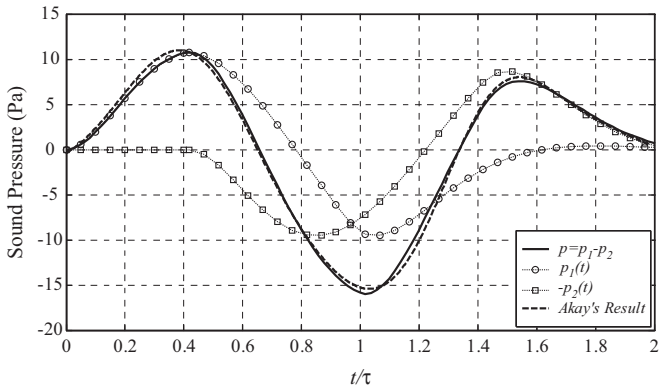

Fig. 2. Sound pressure wave for the impact of a sphere with reflecting plane (r=0.7 m, $\theta=\pi/4$, a=19.05 mm, m=40.5 g, U_0=1.4 m/s and $K_{HZ}=5.6\times10^8$ N/m$^{1.5}$).

The time delay between the sound wave radiated from each image and the main mass can be formulated as follows:

$$T_d^{1-2}=\frac{|r_2-r_1|}{c} \quad , \quad T_d^{1-3}=\frac{|r_3-r_1|}{c} \quad , \quad T_d^{1-4}=\frac{|r_4-r_1|}{c} \quad (23)$$

Table 1
Values of sound pressure level for the impact of Acrylic sphere with steel plane (r=28.28 cm, $\theta=\pi/4$).

a (mm)	U_0 (m/s)	*SPL* (dB) Experimental results [15]	*SPL* (dB) Theoretical results	Error (%)
9.525	0.99	104	97.7250	6.03
9.525	1.40	110	101.7199	7.53
9.525	1.98	113	105.6079	6.54
9.525	2.80	116	109.3810	5.71
19.05	0.99	110	101.3914	7.83
19.05	1.40	113	105.6063	6.54
19.05	1.98	118.5	109.7315	7.40
19.05	2.80	121	113.7236	6.01

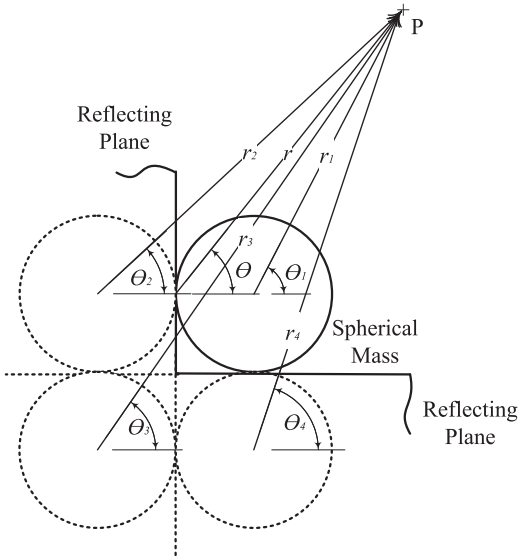

Fig. 4. Quadrupole and its images representation of the wall–floor intersection impact problem.

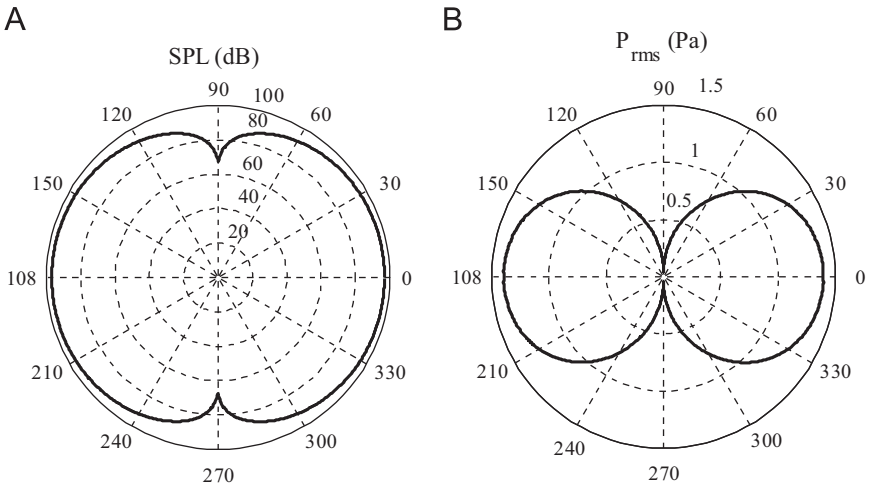

Fig. 3. Theoretical directive *SPL* (A) and root mean square pressure (B), radiated from the dipole.

where superscript $(1-i)$ represents the time delay between the sound pressure waves which are radiated from the main mass and the ith image. Sound pressure radiated from the quadrupole source is shown in Fig. 5 and the directivity pattern for the source is shown in Fig. 6.

At here it should be remembered that the directivity index (DI) for a point source placed on a perfectly reflecting plane is equal to 3 dB. For a point source located at the junction of a vertical perfectly reflecting wall with a horizontal perfectly reflecting plane, the directivity index is equal to 6 dB. In logarithmic form, the relationship between sound pressure level (SPL) and the sound power (L_W) can be written as follows [20]:

$$SPL = L_W + DI - 20\log r - 11 \text{ dB} \quad (24)$$

If the impact occurs near reflecting plane or near wall–floor intersection, the sound power does not change but the directivity index changes from 3 dB to 6 dB [20]. Therefore, regarding to Eq. (24), in same distance from the contact point (r), the difference between the measured sound pressure levels of the quadrupole and the dipole sources should be equal to 3 dB. Note that, close to the source (near field) the sound pressure falls off rapidly, while far from the source (far field) the pressure falls off more slowly. In the far field, the sound pressure and particle velocity are very nearly in phase. The extent of the near field depends on [18,20]:

- The type of source (monopole, dipole, size of machine, type of machine, etc.)
- Frequency of the sound.

The differences between the sound pressure level radiated from the quadrupole and the dipole sources versus the distance from the contact point (r) are plotted in Fig. 7. In this figure, it is shown that difference between the sound pressure level of the quadrupole and the dipole sources, in far field, approaches to 3 dB. The SPL, which is radiated from the dipole source, is verified with the experimental results. Therefore, it can be concluded that the theoretical result, which is calculated for the quadrupole source is acceptable in far field. Error of using the presented theoretical results to model the quadrupole source versus the variable r is shown in Fig. 7.

4. Single unit impact damper

In this section, application of the presented acoustic relations is studied in case of single unit impact dampers. In such systems, the impact occurs near two reflecting planes. Therefore, the impulsive noise generated from the impact dampers, can be modeled using the acoustic relations for the quadrupole type sources, which are presented in previous section.

The impact damper consists of a small loose mass within a main mass that freely moves through an enclosure connected to the main mass. In impact dampers, energy loss in each inelastic contact leads to suppress undesirable vibrations. The dynamic characteristics of the single unit impact dampers can be analyzed using a two-degrees-of-freedom model as shown in Fig. 8. This

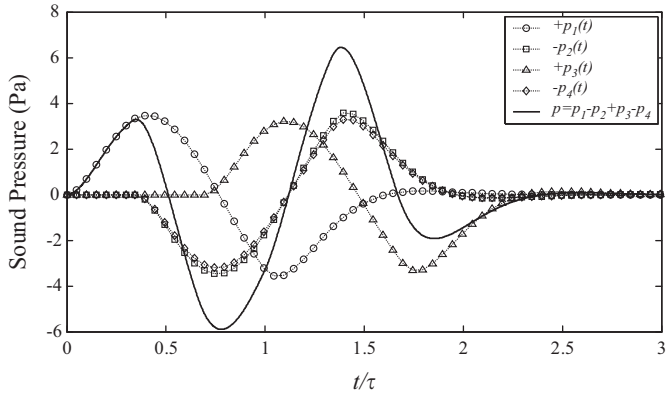

Fig. 5. Sound pressure wave for the impact of a sphere with wall–floor intersection ($r=0.7$ m, $\theta=\pi/4$, $a=19.05$ mm, $U_0=1.4$ m/s and $K_{HZ}=5.6\times10^8$ N/m$^{1.5}$).

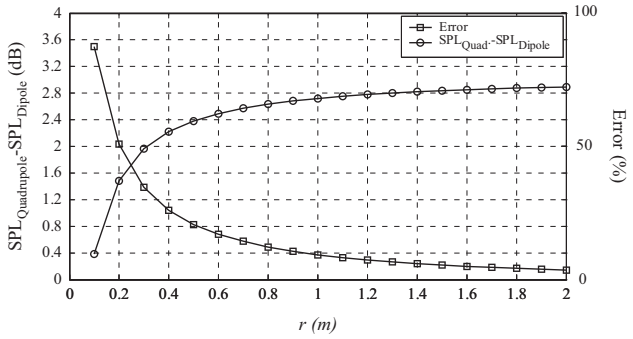

Fig. 7. The difference between values of SPL for the dipole and quadrupole sources at $\theta=\pi/2$ and Error of using the theoretical result.

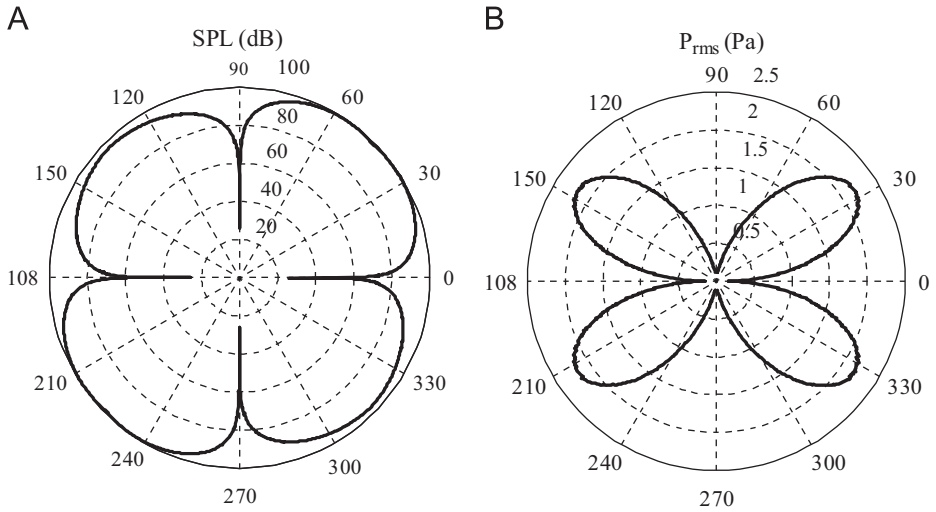

Fig. 6. Theoretical directive SPL (A) and root mean square pressure (B), radiated from the quadrupole.

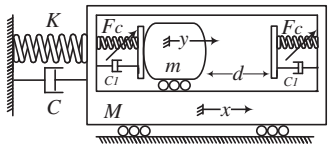

Fig. 8. Schematic figure of a vibratory system equipped with an impact damper ($F_c = K_{HZ} Z^{3/2}$).

model is consisted of an oscillator with linear stiffness K, mass M, viscous damping C and an impact damper with mass m and gap size d.

When the impact mass moves between the barriers, the differential equations for vibratory motion of the impact mass and the main mass, are as follows [5]:

$$M\frac{d^2x}{dt^2} + C\frac{dx}{dt} + Kx = 0$$
$$m\frac{d^2y}{dt^2} = 0 \tag{25}$$

In the present study, the friction force between M and m is neglected. When the impact mass collides with the main mass, an impulsive force acts on both of them. In the present study, the Hertzian contact model presents the impact force between the masses. Consequently, when the impact mass collides with the main mass, the differential equations of motion can be written as follows:

$$M\frac{d^2x}{dt^2} + C\frac{dx}{dt} + Kx = c_1\frac{dz}{dt} + K_{HZ}z^{3/2}$$
$$m\frac{d^2y}{dt^2} + c_1\frac{dz}{dt} + K_{HZ}z^{3/2} = 0 \tag{26}$$

where $z = y - x$ is relative displacement and c_1 is equivalent contact damping constant. Note that, the variable U_0 in the acoustic relations is equal to $\dot{z}(0)$. The values of the model parameters, in the present study, are listed in Table 2.

The Newmark-beta integration method is used to solve Eq. (26), theoretically [21,22]. In the present study, the time step is considered as $\Delta t = 10^{-7}$ s. Decay of maximum displacements in free vibrations of a vibratory system with viscous damping is nearly exponential. However, in the case of a vibratory system that is equipped with an impact damper, the decay of maximum displacements is initially linear and after a considerable decrease in displacement amplitude, it is exponential [6]. The waveforms of free vibrations without and with impact damper are shown in Fig. 9.

The initially linear decrease in the maximum displacement of the vibratory system, which is equipped with an impact damper, is usually represented by damping inclination. The damping inclination is defined as [6]:

$$e = \frac{X_1 - X_2}{t_2 - t_1} \tag{27}$$

where t_1 and t_2 are the times of occurrence of the maximum positive displacements X_1 and X_2, respectively. Variation of the damping inclination with the impact mass and gap size, for the presented vibratory system, is shown in Fig. 10(A). As shown in this figure, the damping inclination does not vary uniformly by changing the impact mass and the gap size. Effects of changing the impact mass and the gap size on the maximum value of the *SPL* radiated from the impact damper is shown in Table 3.

Unlike the damping inclination, which is depicted in Fig. 10, the maximum sound pressure level varies relatively uniform with changing the impact mass and the gap size. The uniform variation of the maximum sound pressure level is shown in Fig. 11.

Table 2
Parameters for the vibratory system with an impact damper.

$C = 0.05$ N S/m	$K = 500$ N/m
$c_1 = 20$ N S/m	$K_{HZ} = 5.6 \times 10^8$ N/m$^{1.5}$
$M = 0.5$ kg	$m = 40.5$ g

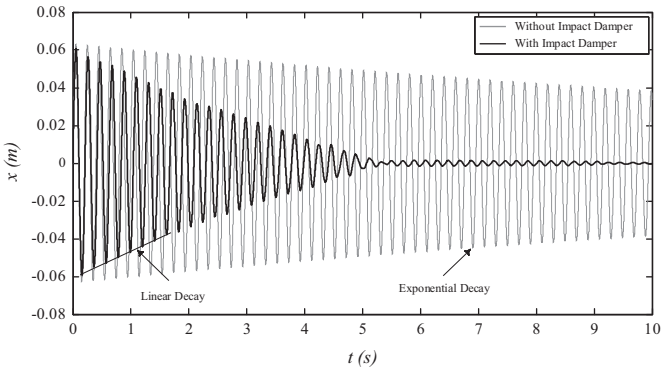

Fig. 9. Waveforms of free vibrations without and with impact damper ($\dot{x}_0 = 2$ m/s and $d = 4$ cm).

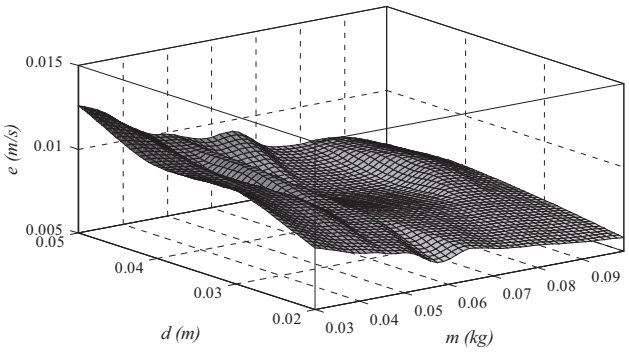

Fig. 10. Variation of the damping inclination with the gap size and the impact mass ($M = 0.5$ kg).

Table 3
Maximum values of the relative velocity and the sound pressure level at $r = 0.7$ m ($M = 0.5$ kg).

M (kg)	$d = 2$ cm		$d = 3$ cm		$d = 4$ cm		$d = 5$ cm	
	U_{0max} (m/s)	SPL_{max} (dB)	U_{0max} (m/s)	SPL_{max} (dB)	U_{0max} (m/s)	SPL_{max} (dB)	U_{0max} (m/s)	SPL_{max} (dB)
0.0298	1.4000	99.48	1.6115	101.01	1.8793	103.07	2.1112	104.54
0.0345	1.4000	99.49	1.6115	101.35	1.8741	103.32	2.1026	104.84
0.0396	1.4000	99.82	1.6107	101.68	1.8877	103.74	2.1126	105.23
0.0452	1.4000	100.14	1.6262	102.11	1.8796	104.02	2.1008	105.50
0.0513	1.4000	100.46	1.6219	102.39	1.8889	104.38	2.1065	105.63
0.0579	1.4000	100.76	1.6326	102.77	1.8766	104.62	2.1094	105.95
0.0650	1.4000	101.06	1.6239	103.01	1.8806	104.95	2.0908	106.16
0.0728	1.4000	101.36	1.6295	103.35	1.8820	104.91	2.0886	106.44
0.0811	1.4031	101.67	1.6328	103.66	1.8632	105.09	2.0841	106.71
0.0900	1.4092	102.00	1.6348	103.96	1.8612	105.36	2.0781	106.96
0.0995	1.4038	102.24	1.6369	104.25	1.8592	105.63	2.0719	107.21

As shown in Table 1, the sound pressure level relates to the contact velocity (U_0) and radius of the impact mass (a). Increasing mass of the impact mass and the gap size leads to increase the radius of the impact mass and increase the contact velocity, respectively. Therefore, as shown in Fig. 11, rising the impact

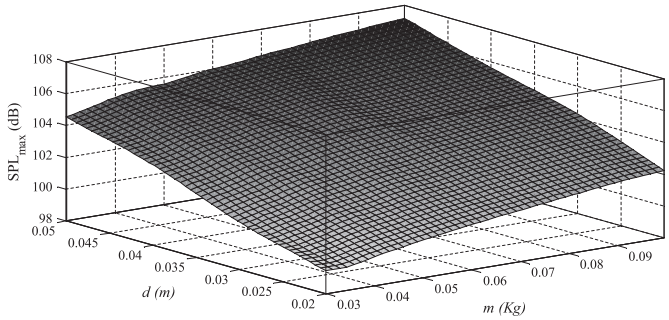

Fig. 11. Variation of the maximum sound pressure levels with impact mass and gap size (M=0.5 kg).

mass and gap size leads to increase the maximum sound pressure level.

5. Results and discussion

A theoretical model to predict the sound pressure wave generated from the elastic contact of a spherical mass with a reflecting plane has been developed. The impact force is modeled using the Hertzian contact theory. The theoretical model for the dipole acoustic source and the corresponding experimental results are compared to verify the theoretical results. Comparison of theoretical results with previous experimental results is shown in Fig. 2 and Table 1. The sound pressure, radiated from a quadrupole source, is achieved using the method of images. Effect of varying the distance between the measurement point and the contact point (r) on the sound pressure radiated from the quadrupole source is shown in Fig. 12.

A vibratory mass equipped with a single unit impact damper is modeled using a nonlinear two-degree-of-freedom system. The coupled differential equations of the system are solved using the Newmark-beta integration method. To verify the calculated results, the contact duration, which is obtained using the Newmark-beta method, are compared with the previous exact results [17]. Comparison of theoretical results with the exact solution is shown in Table 4.

Unlike usual method to study the impact dampers, in the present study, the coefficient of restitution varies with the impact mass. Variation of the coefficient of restitution versus the impact mass is shown in Fig. 13.

Effect of varying the gap size and impact mass on the damping inclination is shown in Fig. 14. As shown in this figure, for m between 30 g and 100 g, the damping inclination decreases when the impact mass increases. Furthermore, in this figure it is shown that the damping inclination for small values of the gap size decreases relatively uniform.

Contour plot of the damping inclination with the impact mass and the gap size is illustrated in Fig. 15. In this figure, it is clearly shown that the damping inclination does not vary uniformly with changing the impact mass and the gap size. Generally, the impact dampers are designed for strongly suppressing undesired vibrations. In the present study, the design method will be improved by considering the acoustic behavior of the impact dampers. Relatively uniform variation of the maximum sound pressure level with the impact mass and the gap size is depicted in Fig. 16.

Hence, it can be concluded that the design of an impact damper may be divided to two parts. The first one refers to select the parameters of impact dampers to suppress undesired vibrations, rapidly. This kind of design can conveniently be named as "vibration-based" design. Another design method is based on how to design a low noise system. This kind of design method can be

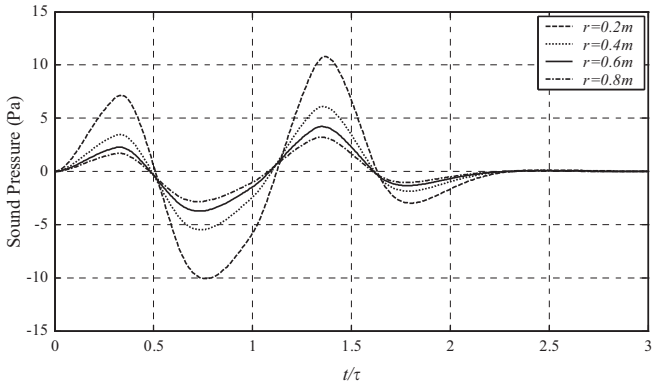

Fig. 12. Variation of the sound pressure with the dimensionless time by changing the parameter r ($\theta=\pi/4$, a=19.05 mm, U_0=1.4 m/s and $K_{HZ}=5.6\times10^8$ N/m$^{1.5}$).

Table 4
Comparison of theoretical result and exact solution (m=40 g and M=0.5 kg).

U_0 (m/s)	Newmark-beta i ntegration method	Exact solution [17]	Error (%)
1.3	0.000259	0.000260	0.095
1.4	0.000256	0.000256	0.106
1.5	0.000253	0.000253	0.095
1.6	0.000250	0.000250	0.193
1.7	0.000247	0.000247	0.198
1.8	0.000245	0.000244	0.530
1.9	0.000242	0.000241	0.378
2.0	0.000240	0.000239	0.575
2.1	0.000238	0.000236	0.715
2.2	0.000236	0.000234	0.802

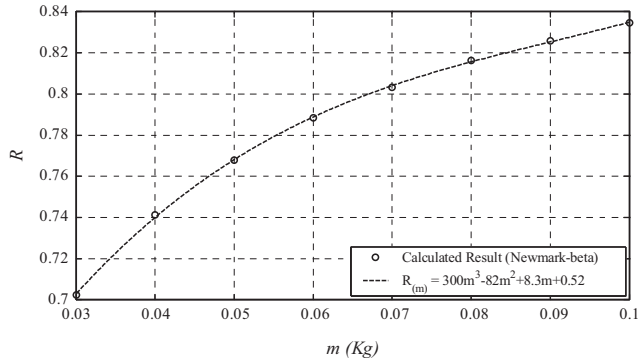

Fig. 13. Variation of the coefficient of restitution versus the impact mass (M=0.5 kg).

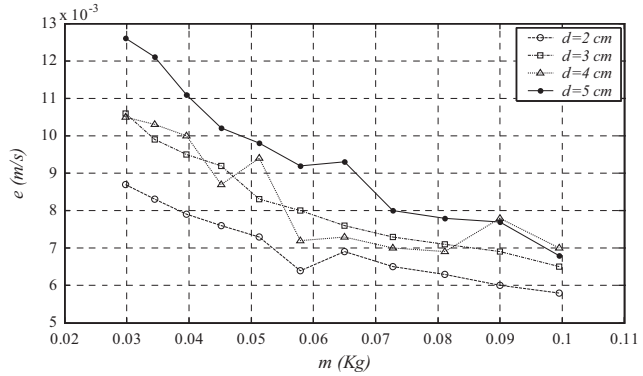

Fig. 14. Variation of the damping inclination versus the impact mass (M=0.5 kg).

named as "acoustic-based" design. Combining the acoustic-based and the vibration-based design leads to make a perfect impact damper. Fig. 17 provides a useful chart to combine the discussed design methods. As shown in this figure, for some values of the damping inclination, the maximum sound pressure level varies up to 8 dB. This figure can be divided to four zones, which are shown in the figure. The impact damper in zone1 is a noisy system, which is not suitable for suppressing undesired vibrations. In zone2, the impact damper is a noisy system, which can strongly suppress vibrations. Selecting the gap size and mass ratio in zone4 provides a relatively low noise impact damper, which cannot strongly suppress vibrations. In comparison to the other zones, the design parameters for a low noise and powerful impact damper are located in zone3. In other words, if the gap size is selected between 2 cm and 3 cm and the impact mass is selected between 30 g and 60 g, both of the vibration-based and the acoustic-based considerations can relatively be satisfied.

Extent of the maximum *SPL* in each value of the damping inclination is shown in Table 5. It can be concluded that if the damping inclination varies between 0.7 cm/s and 1.1 cm/s, the acoustic-based consideration can decrease the sound pressure level between 4 dB and 8 dB.

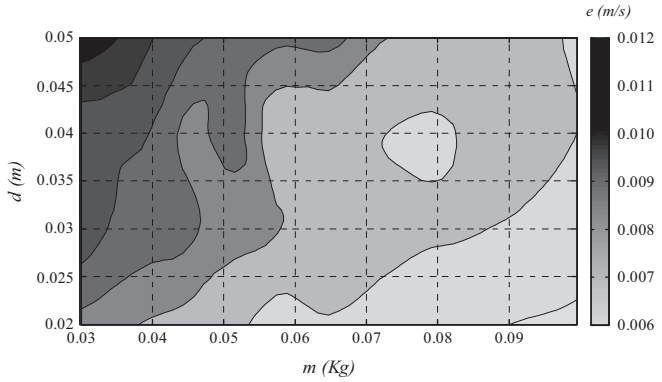

Fig. 15. Variation of the damping inclination with the impact mass and the gap size (M=0.5 kg).

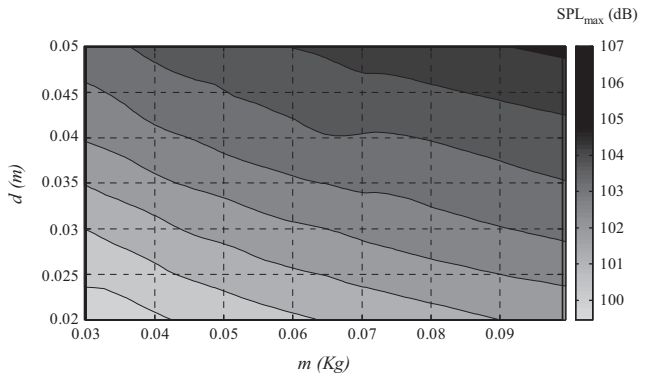

Fig. 16. Variation of the maximum sound pressure level with the impact mass and the gap size (M=0.5 kg).

6. Conclusion

An analytical model has been used to predict the sound pressure waveform radiated from the impact of a spherical mass with a reflecting plane and wall–floor intersection. The theoretical results are verified with the previous experimental measurements. The acoustic noises generated by impact dampers are calculated using the theoretical results.

Dynamic behavior of the vibro-impact system is presented using a nonlinear model that incorporates the Hertzian contact theory. The nonlinear differential equations are solved theoretically using the Newmark-beta method. It is clearly shown that the theoretical solutions are in close agreement with the previous exact results.

Effects of varying the mass ratio and the gap size have been studied on the dynamic and acoustic behavior of a vibratory system equipped with the impact damper. It is shown that, unlike the damping inclination, the maximum sound pressure level that is generated by the impact damper, varies uniformly with the gap size and the mass ratio. The vibration-based and the acoustic-

Table 5
Extent of the maximum *SPL* in each value of the damping inclination.

SPL (dB)→ *e* (cm/s)↓	100	101	102	103	104	105	106	107	108
0.7									
0.8									
0.9									
1.0									
1.1									
1.2									

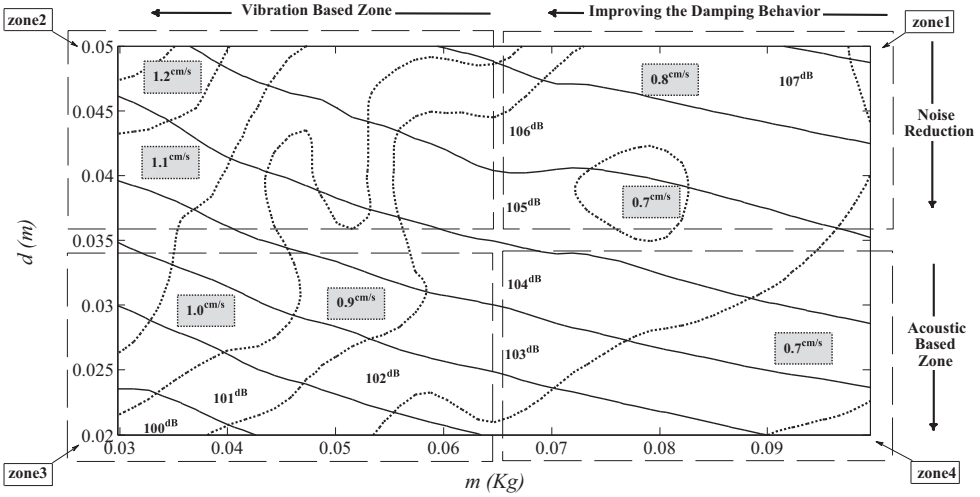

Fig. 17. Variation of maximum *SPL* and the damping inclination with m and d for M=0.5 kg (– and · · · · · · indicate *SPL* and damping inclination margins, respectively).

based design of an impact damper are combined in a user-oriented chart to find a low noise and strong impact damper. Finally, it is shown that for a relatively extensive range of the damping inclination, the acoustic-based consideration decreases the sound pressure level up to 8 dB.

References

[1] Babitsky VI. Theory of vibro-impact systems and applications. Berlin; New York: Springer; 1998.
[2] Stronge WJ. Impact mechanics. Cambridge, England; New York: Cambridge University Press; 2000.
[3] Blazejczyk-Okolewska B. Analysis of an impact damper of vibrations. Chaos, Solitons Fractals 2001;12:1983–8.
[4] Zhang D-G, Angeles J. Impact dynamics of flexible-joint robots. Comput Struct 2005;83:25–33.
[5] Cheng J, Xu H. Inner mass impact damper for attenuating structure vibration. Int J Solids Struct 2006;43:5355–69.
[6] Bapat CN, Sankar S. Single unit impact damper in free and forced vibration. J Sound Vib 1985;99:85–94.
[7] Ema S, Marui E. A fundamental study on impact dampers. Int J Mach Tools Manuf 1994;34:407–21.
[8] Cheng CC, Shiu JS. Transient vibration analysis of a high-speed feed drive system. J Sound Vib 2001;239:489–504.
[9] Cheng CC, Wang JY. Free vibration analysis of a resilient impact damper. Int J Mech Sci 2003;45:589–604.
[10] Du Y, Wang S. Modeling the fine particle impact damper. Int J Mech Sci 2010;52:1015–22.
[11] Ibrahim RA. Vibro-impact dynamics: modeling, mapping and applications. Berlin: Springer Verlag; 2009.
[12] Macaulay M. Introduction to impact engineering. London; New York: Chapman and Hall; 1987.
[13] Fahy F, Gardonio P. Sound and structural vibration: radiation, transmission and response. 2nd ed. Amsterdam; Boston: Elsevier/Academic; 2007.
[14] Koss LL, Alfredson RJ. Transient sound radiated by spheres undergoing an elastic collision. J Sound Vib 1973;27:59–68 IN51-IN52, 69-75.
[15] Akay A, Hodgson TH. Acoustic radiation from the elastic impact of a sphere with a slab. Appl Acoust 1978;11:285–304.
[16] Yufang W, Zhongfang T. Sound radiated from the impact of two cylinders. J Sound Vib 1992;159:295–303.
[17] Goldsmith W. Impact: the theory and physical behaviour of colliding solids. Mineola, N.Y.: Dover Publications; 2002.
[18] Wilson CE. Noise control,. Malabar, FL: Krieger; 2005.
[19] Morse PM. Vibration and sound. New York: American Institute of Physics for the Acoustical Society of America; 1981.
[20] Crocker MJ. Handbook of noise and vibration control. Hoboken, N.J.: John Wiley; 2007.
[21] Afsharfard A, Farshidianfar A. An efficient method to solve the strongly coupled nonlinear differential equations of impact dampers. Arch Appl Mech 2012;82:977–84.
[22] Clough RW, Penzien J, Dynamics of structures, 2nd ed., Comput Struct, Berkeley, Calif., 2010.